PB86-117371

Advanced Electrostatic Enhancement of Fabric Filtration

Research Triangle Inst.
Research Triangle Park, NC

Prepared for

Environmental Protection Agency
Research Triangle Park, NC

Oct 85

U.S. Department of Commerce
National Technical Information Service
NTIS

PE86-117371

EPA/600/D-85/267
October 1985

ADVANCED ELECTROSTATIC ENHANCEMENT OF FABRIC FILTRATION

Ronald B. Mosley, Louis S. Hovis, Norman Plaks

Air and Energy Engineering Research Laboratory
U. S. Environmental Protection Agency
Research Triangle Park, North Carolina 27711

and

Toshiaki Yamamoto, Andrew S. Viner, David S. Ensor

Center for Aerosol Technology
Research Triangle Institute
Research Triangle Park, North Carolina 27709

CR812281-01

EPA Project Officer
Ronald B. Mosley

AIR AND ENERGY ENGINEERING RESEARCY LABORATORY
OFFICE OF RESEARCH AND DEVELOPMENT
U.S. ENVIRONMENTAL PROTECTION AGENCY
RESEARCH TRIANGLE PARK, NC 27711

REPRODUCED BY
NATIONAL TECHNICAL
INFORMATION SERVICE
U.S. DEPARTMENT OF COMMERCE
SPRINGFIELD, VA 22161

TECHNICAL REPORT DATA
(Please read Instructions on the reverse before completing)

1. REPORT NO. EPA/600/D-85/267	2.
3. RECIPIENT'S ACCESSION NO. PB86 117371/AS	
4. TITLE AND SUBTITLE Advanced Electrostatic Enhancement of Fabric Filtration	5. REPORT DATE October 1985
	6. PERFORMING ORGANIZATION CODE
7. AUTHOR(S) R. B. Mosley, L. S. Hovis, and N. Plaks (EPA); and T. Yamamoto, A. S. Viner, and D. S. Ensor (RTI)	8. PERFORMING ORGANIZATION REPORT NO.
9. PERFORMING ORGANIZATION NAME AND ADDRESS Research Triangle Institute P. O. Box 12194 Research Triangle Park, North Carolina 27709	10. PROGRAM ELEMENT NO.
	11. CONTRACT/GRANT NO. CR812281-01
12. SPONSORING AGENCY NAME AND ADDRESS EPA, Office of Research and Development Air and Energy Engineering Research Laboratory Research Triangle Park, NC 27711	13. TYPE OF REPORT AND PERIOD COVERED Published Paper; 10/85
	14. SPONSORING AGENCY CODE EPA/600/13

15. SUPPLEMENTARY NOTES AEERL project officer is Ronald B. Mosley, Mail Drop 61, 919/541-7865.

16. ABSTRACT The paper discusses laboratory and pilot plant studies of a modification of the U. S. EPA's Electrically Stimulated Fabric Filtration (ESFF) method in which corona voltage on a center-wire electrode replaces the subcorona electrodes at the bag surface. The electric field which affects enhancement results from the high potential maintained on the center wire. The mechanism that supports the observed increase in gas flow consistent with the theoretical model involves the nonuniform deposition of the charged dust as a result of forces exerted on the particles in the electric field perpendicular to the bag. Laboratory results show an extremely low rate of pressure drop increase during the filtration cycle, only 10-30% of the rate associated with conventional reverse-air fabric filtration. Pilot plant data indicate a corresponding increase in flow through electrified bags. The rudiments of a mathematical model for describing the electrical deposition of the dust are presented.

17. KEY WORDS AND DOCUMENT ANALYSIS

a. DESCRIPTORS		b. IDENTIFIERS/OPEN ENDED TERMS	c. COSATI Field/Group	
Pollution	Fabrics	Pollution Control	13B	11E
Flue Gases	Mathematical Models	Stationary Sources	21B	12A
Dust		Electrically Stimulated Fabric Filtration	11G	
Particles			14G	
Electrostatics		Particulate	20C	
Filtration		Fabric Filters	07D	

18. DISTRIBUTION STATEMENT Release to Public	19. SECURITY CLASS (This Report) Unclassified	21. NO. OF PAGES 24
	20. SECURITY CLASS (This page) Unclassified	22. PRICE

EPA Form 2220-1 (9-73)

NOTICE

This document has been reviewed in accordance with U.S. Environmental Protection Agency policy and approved for publication. Mention of trade names or commercial products does not constitute endorsement or recommendation for use.

ABSTRACT

Laboratory and pilot plant studies have been conducted on a modification of U. S. Environmental Protection Agency's Electrically Stimulated Fabric Filtration (ESFF) method in which corona voltage on a center-wire electrode replaces the subcorona electrodes at the bag surface. The electric field which affects enhancement results from the high potential maintained on the center wire. The mechanism that supports the observed increase in gas flow consistent with the theoretical model involves the nonuniform deposition of the charged dust as a result of forces exerted on the particles in the electric field perpendicular to the bag. Laboratory results show an extremely low rate of pressure drop increase during the filtration cycle, only 10 to 30 percent of the rate associated with conventional reverse-air fabric filtration. Pilot plant data indicate a corresponding increase in flow through electrified bags. The rudiments of a mathematical model for describing the electrical deposition of the dust are presented.

ADVANCED ELECTROSTATIC ENHANCEMENT OF FABRIC FILTRATION

Ronald B. Mosley, Louis S. Hovis, Norman Plaks,*
Toshiaki Yamamoto, Andrew S. Viner, and David S. Ensor**

INTRODUCTION

The ability of an electrically stimulated fabric filter (ESFF) to operate at a lower average pressure drop than a conventional fabric filter has been successfully demonstrated in the laboratory and in two pilot plant studies with pulverized coal ashes (1,2,3). Those investigations involved the use of an electric field oriented parallel to the surface of the bag fabric. The presence of the electric field produced a dust cake with a lower pressure drop than when no electric field was present. There was no statistically significant difference in the mass emissions between the electrified and nonelectrified cases.

In recent laboratory investigations, a high voltage wire was placed in the center of the bag tube to produce an electric field that was perpendicular (rather than parallel) to the surface of the fabric. This "center-wire" configuration produced even more impressive pressure reductions than the parallel field case. The center-wire configuration offers an important additional advantage over the parallel-field configuration in the case of carbon-rich (i.e., low resistivity) ashes such as are sometimes emitted from stoker-fired boilers. In a parallel-field bag, the electrodes are in contact with the bag fabric; consequently, a dust with high electrical resistance helps prevent shorts that could cause distortions of the electric field and possibly burn holes in the bag. The resistivity of ashes from stoker-fired boilers is sometimes lower than that from pulverized-coal-fired boilers due to the higher carbon content of the stoker ash. The parallel field ESFF is,

*Air and Energy Engineering Research Laboratory, U. S. Environmental Protection Agency, Research Triangle Park, North Carolina 27711.

**Center for Aerosol Technology, Research Triangle Institute, P. O. Box 12194, Research Triangle Park, North Carolina 27709.

therefore, less likely to show an advantage over conventional fabric filtration for that type of ash because the low resistivity tends to reduce the effectiveness of the electric field in the dust cake. In addition, the relatively high conductivity of the ash means that the dust layer on the bag can serve as the ground surface for the electric potential when a center wire is used.

It is not intended to suggest that the advanced (center-wire) ESFF geometry will work only with high conductivity ashes. The center-wire configurations have, in fact, been successfully applied to higher resistivity ashes at EPA's laboratory facilities.

In conjunction with both laboratory and pilot studies, a mathematical model has been developed to predict the role of basic parameters on particle motion and dust deposition distributions. Those parameters are reduced to one dimensionless parameter, the ES number, which represents the effectiveness of electrostatic augmentation on the ESFF configuration. The particle motion and particle deposition distribution are evaluated by using the ES number.

Both the empirical results and the mathematical model show an extreme reduction in the pressure drop during the filtration cycle when compared with the conventional reverse-air fabric filtration. This suggests that a higher A/C could be used without sacrificing overall pressure drop.

EXPERIMENTAL STUDY

The pilot work described here uses a center-wire geometry as shown in Figure 1 for collecting the high carbon ash from a stoker-fired boiler. The pilot plant operates on a slipstream from two stoker-fired boilers which burn eastern coals to generate a maximum of 77,000 lb/h of steam. This pilot plant consists of one compartment containing up to six bags, both ESFF and conventional bags, with a maximum flue gas flow rate of 600 acfm. Each bag is 8 in. in diameter and 24 ft in length.

In earlier studies of ESFF geometries (2,3) two side-by-side compartments were used: one compartment was outfitted with ESFF; and the other, as a standard baghouse to serve as an experimental control. It was assumed that all of the bags in a compartment were identical in their operation. The overall compartment pressure drop and flow rate were used to monitor compartment performance. There was no way to know whether or not all of the bags were in fact

performing the same way. The ability to monitor individual bag performance would greatly enhance confidence in the ESFF concept. Toward this goal, a new method of baghouse monitoring was used in this study to quickly and reliably evaluate the electrostatically augmented filtration technique. For this evaluation, each bag was fitted with a calibrated orifice (called an Individual Bag Flow Monitor, or IBFM) to measure the gas flow rate into the bag. This flow rate information, coupled with the known pressure drop across the tubesheet of the baghouse, is used to compute the flow resistance (drag):

$$S = P/V_0 \quad , \tag{1}$$

where: S = flow resistance (drag) (Pa s/m),
P = tubesheet pressure drop (Pa), and
V_0 = face velocity through bag (= flow rate/bag area) (m/s).

The drag is directly related to the amount of dust on the fabric by the relation:

$$S = S_e + K_2 W \quad , \tag{2}$$

where: S_e = effective flow resistance after cleaning (Pa s/m),
K_2 = specific resistance coefficient (N s/kg m), and
W = dust mass per unit area (kg/m^2).

The mass per unit area (W) can be estimated from the relation:

$$W = C_i \int_0^t V_0 \, dt \quad , \tag{3}$$

where: C_i = inlet dust concentration (measured, and assumed to remain constant)(kg/m^3).

Figure 2 is representative of the data collected at the ESFF pilot plant. The face velocities shown in the figure were calculated from measurement of individual bag flows. The two upper curves in the figure show the flow of the ESFF bags increasing with time, whereas the conventional bags (the lower curves) have a decreasing flow with time. Based on the flow information contained in Figure 2 and a known inlet dust concentration, the dust load on a

bag (mass per unit area) can be calculated as a function of time (Equation 3). In addition, from the known flow information and tubesheet pressure drop data, the drag across each bag can be calculated as a function of time (Equation 1). A common assumption of baghouse modeling is that the drag across a bag is a linear function of the amount of dust on the bag (Equation 2). This linear model is characterized by the rate of drag increase, called the dust cake specific resistance (K_2), and the drag at zero dust load, called the residual drag (S_e). Figures 3 and 4 show the drag behavior for an ESFF and a nonESFF bag, respectively. The straight lines in the figures are the regression fits to the data (Equation 2). The results of the regression analysis are summarized in Table 1. In short, the pilot plant data indicate that the drag (and, hence, the pressure drop) across an ESFF bag rises at less than one fifth the rate of a conventional bag. In addition, an ESFF bag has a lower drag (and pressure drop) after cleaning. These benefits are important from two perspectives. For the operator of an existing baghouse, the addition of the advanced ESFF system will mean lower pressure drops. Economic feasibility will depend, of course, on the severity of the existing pressure drop problem. For the engineer considering the construction of a new baghouse, the inclusion of ESFF hardware in the design will mean that a smaller (and less expensive) baghouse can be specified.

Table 1.

DRAG VERSUS DUST LOAD REGRESSION RESULTS

	Bag No. 1 (ESFF)	Bag No. 2 (Conventional)
Specific resistance (K_2) [in. H_2O/(ft/min x lb/ft^2)]	0.977	5.873
Residual Drag (S_e) (in. H_2O/ft/min)	0.259	0.287

MATHEMATICAL MODEL

Figure 5 illustrates the advanced ESFF configuration where the flow comes from the bottom and leaves to the side. First, the flow field in the bag filter is determined. The charge on the particles is calculated next. At this point,

both the electric field strength and the velocity of an individual particle moving toward the filter surface (within the active region) are obtained. The final steps consist of calculating the particle trajectories and determining the dust deposition distribution.

Gas Streamlines

In order to determine the flow field, one must solve the Navier-Stokes equation with appropriate boundary conditions. However, any analytical solution satisfying the boundary conditions and appearing reasonable is assumed to be similar to the solution of the Navier-Stokes equation. This is especially true with large aspect ratios [ratio of filter length (L) to filter radius (R)]. Figure 5 shows the coordinate system for the advanced ESFF configuration. Assuming uniform distributions of inlet and outlet flow velocities (U_0 and V_0, respectively), the intercepting points z_i for the gas streamline (ψ_i, starting at the position r_i) can be determined by applying mass conservation:

$$z_i = L - \left(\frac{U_0}{V_0}\right) \frac{r_i^2}{2R} = L\left[1 - \left(\frac{r_i}{R}\right)^2\right] \quad . \tag{4}$$

The spatial position (r, z) for a given streamline (ψ_i) is assumed to follow a super elliptic equation, represented by:

$$r = R\left\{1 - \left[1 - \left(\frac{r_i}{R}\right)\right]\left[1 - \left(\frac{z}{z_i}\right)^n\right]^{1/n}\right\}_{\psi_i} \quad . \tag{5}$$

The value n = 2 is selected for all r_i and z_i such that the flow field appears reasonable. The radius at the filter inlet is divided into 10 segments (i = 10), and L is divided into 40 segments in the z direction.

Particle Charging

For field charging theory, the charge on a nonconductive particle [q(t)] is given as a function of time:

$$q(t) = q_s \frac{1}{(1 + \tau/t)} \quad , \tag{6}$$

where: $q_s = 12\pi \frac{k}{(k + 2)} \varepsilon_0 a^2 E_0$,

$$\tau = \frac{4\varepsilon_0}{K\rho} = \frac{4\varepsilon_0 E_0}{J} \quad , \tag{7}$$

and: q_s = saturation charge,
$E_0 = V_0/R$ = average field,
V_0 = applied voltage,
J = current density,
k = relative dielectric constant,
ε_0 = permittivity of vacuum,
a = particle radius,
ρ = ionic space charge density, and
K = ion mobility.

For typical ESFF operation with a dielectric particle ($E_0 = 3.0 \times 10^5$ V/m, $J = 1 \times 10^{-4}$ A/m^2), the time constant (τ) becomes 0.1 s from Equation 7. Since the charging time (t) is several times greater than τ, it is reasonable to assume that the charge on the particles is close to that of the saturation charge (q_s).

Particle Mobility

Newton's law governs the motion of a charged particle under the influence of an electric field. If the particle inertia is ignored, one obtains the particle migration velocity (V_p) by balancing the electrical force and viscous drag forces:

$$V_p = \frac{C\, q\, E}{6\pi\, \eta\, a} = K_p\, E \quad . \tag{8}$$

Therefore, the particle mobility (K_p) can be written as:

$$K_p = \frac{q\, C}{6\pi\, \eta\, a} = \frac{2\varepsilon_0\, k\, a\, C\, E_0}{(k+2)\eta} = f\,(E_0, a, \eta) \quad , \tag{9}$$

where: C(C = 1.0) = Cunningham slip coefficient, and
η = viscosity of the gas.

Therefore, the particle mobility becomes a function of a and E_0 for known gas thermodynamic properties.

Electric Field

Due to axial symmetry, the electric field equation for wire-cylinder electrodes reduces to a one-dimensional problem if end effects are ignored. In neglecting the ionic space charge, the electric field at any radius E(r) can be determined from the relationship:

$$E(r) = \frac{V_0}{r \ln (R/r_a)} \quad , \tag{10}$$

where r_a = the radius of the discharge wire. The local migration velocity of the charged particle [$V_p(r, z)$] is obtained by substituting Equations 10 and 9 in Equation 8.

Particle Trajectories

Figure 6 shows both the gas (ψ_i) and particle (Φ_i) streamlines, starting at the position r_i. The position (r', z') for Φ_i can be expressed as the position designated in the previous increment by (n - 1) of ψ_i and V_p:

$$\left(r_n'\right)_{\Phi_i} = \left[r_{n-1}' + \frac{\Delta z}{w_{n-1}} V_{p_{n-1}} + \left(r_n - r_{n-1}\right)\right] \quad . \tag{11}$$

The gas velocity in the z direction [w(r,z)] can be obtained from the gas streamlines. This velocity varies from $w(r, 0) = U_0$ at the filter inlet to $w(R, z) = 0$ at the outlet, while gas velocity in the r direction varies from $v_r(r, 0) = 0$ to $v_r(R, z) = V_0$. Therefore, w(r, z)for a given ψ_i at location n in the z direction is expressed as:

$$w_n = w_{n-1} \left[1 - \left(\frac{r_n - r_{n-1}}{R - r_n}\right)\right]_{\psi_i} \quad . \tag{12}$$

Dust Deposition Distribution

Once the particle trajectories have been determined, the local dust layer thickness can be calculated. Assuming that flow streamlines are not disturbed by the dust deposit during the time interval, the distribution of relative dust layer thickness is determined by the ratio of adjacent gas streamlines to particle streamlines:

$$l_i = \left(\frac{z_{\psi_i} - z_{\psi_{i-1}}}{z_{\phi_i} - z_{\phi_{i-1}}} \right)_{r=R} \quad . \tag{13}$$

One way to verify the simulation is to check the mass conservation (sum of relative thickness multiplied by incremental distance).

RESULTS AND DISCUSSION

The simulations were performed using the Lotus 1-2-3 spreadsheet. Seven basic parameters of data entry yield a nearly instantaneous graphic display of streamlines and particle trajectories. The fundamental relationship among the seven variables can be related to three basic parameters such as r_a, K_p, and A/C:

$$f\left(V_0, r_a, R, L, a, \eta, Q\right) = f\left(r_a, K_p, A/C\right) = 0 \quad . \tag{14}$$

The filtration performance generally is enhanced by reducing A/C and increasing K_p and r_a. As the radius of the wire decreases, the field near the corona wire increases; but it decreases near the bag filter surface. This results in negligible effects on particle trajectories. Since the particle trajectory is barely affected by r_a, the particle spatial behavior can be described by one dimensionless parameter, ES number (N_{ES}). This is defined as:

$$N_{ES} = \frac{K_p E_0}{A/C} = g\left(\frac{a E_0^2 L}{U_0 R \eta} \right) \quad . \tag{15}$$

where g is a constant.

N_{ES}, which includes six of the fundamental parameters discussed above, determines the effectiveness of electrostatic enhancement for the ESFF configuration. In other words, the ES number describes the ratio of average particle migration velocity to the filter face velocity. The higher the ES number, the higher is the effect of electrostatic enhancement. One can see from Equation 9 or 15 that direct enhancement is achieved by increasing a, E_0, and L and decreasing U_0, R, and η.

When A/C = 4.0 ft/min, V_0 = 23 kV, R = 4 in., L = 24 ft, T = 150° C, $2r_a$ = 3.2 mm, and a = 2.0 μm, then N_{ES} becomes 3.57. Figure 7 illustrates both gas

and particle streamlines. In the absence of an electric field, the particle trajectories remain the same as the gas streamlines. Note that the relative radius is chosen to be 0 at the filter surface and 1.0 at the center of the filter. As can be seen from the figure, an electric field considerably influences the charged particle trajectories. The trajectory model remains valid as long as the current density is high enough to achieve saturation charging, the areal density is low enough not to disturb the gas flow, and the particle has a high mobility.

Figure 8 shows the fraction of the dust-free area (A_f) as a function of N_{ES}, resulting in the following relationship:

$$A_f = 1 - \exp\left(-0.117N_{ES}\right) \quad . \tag{16}$$

Figure 9 plots the relative dust deposition distribution as a function of particle size (a = 0.5 μm, a = 2.0 μm, a = 4.0 μm, and a = 8.0 μm). The corresponding values of N_{ES} are 0.89, 3.57, 7.14, and 14.28. When the electric field is not present, the relative deposition thickness becomes uniform (1.0). As a (or N_{ES}) increases, the deposition pattern moves toward the bag filter inlet. Note that the maximum deposition occurs immediately adjacent to the dust-free region. The total mass in these maxima is relatively small, especially for small particles.

Remember, however, that these relative layer thicknesses are computed for single particle sizes. Note that the average layer thickness increases toward the bag inlet for larger particles. Figure 10 shows a composite layer distribution for a log-normal particle size distribution with a mass median diameter (MMD) of 10 μm. The curve in Figure 10 was computed by summing the contributions to total thickness of each particle size. The individual contributions were obtained by scaling curves similar to those in Figure 9 by the fraction of total mass contained in that particular size band. Although the curve in Figure 10 is approximate, its general shape agrees with laboratory observations of dust deposits formed by advanced ESFF.

Reference 4 reported that, when 10 percent of the area is dust free and the residual stress is low, the overall pressure drop diminishes to a value of 1/10. Based on the example above, the preliminary calculation of pressure drop ratio yields approximately 0.2 which shows good agreement with the laboratory and pilot plant results. This suggests that the A/C could be

increased significantly without sacrificing the pressure drop. The flow modifications due to differential particle deposition and varying areal density should be calculated in order to gain a further understanding of the pressure reduction model. Such a calculation is currently in progress.

CONCLUSIONS

The advanced ESFF model was developed to evaluate the effects of fundamental parameters on particle mobility and pressure drop. The spatial behavior of the charged particle is described successfully by the dimensionless ES number. The significant reduction of overall pressure drop also is demonstrated by the existence of a dust-free area (related to ES number). The A/C could be increased significantly without sacrificing the overall pressure drop. Experimental and pilot studies also support these conclusions, in their range of the parametric studies.

REFERENCES

1. B. Miller, G. Lamb, P. Costanza, D. A. Saville, and M. J. Oak. Studies of Dust Cake Formation and Structure in Fabric Filtration. EPA-600/9-81-023 (NTIS PB83-259986), U. S. Environmental Protection Agency, August 1983.

2. D. W. VanOsdell, M. B. Ranade, G. P. Greiner, and D. F. Furlong. Electrostatic Augmentation of Fabric Filtration: Pulse-Jet Pilot Unit Experience. EPA-600/7-82-062 (NTIS PB83-168625), U. S. Environmental Protection Agency, November 1982.

3. D. W. VanOsdell and D. A. Furlong. Electrostatic Augmentation of Fabric Filtration: Reverse-Air Pilot Unit Experience. EPA-600/7-84-085 (NTIS PB84-230002), U.S. Environmental Protection Agency, August 1984.

4. R. Dennis, R. W. Cass, D. W. Cooper, R. R. Hall, V. Hampl, H. A. Klemm, J. E. Langley, and R. W. Stern. Filtration Model for Coal Fly Ash with Glass Fabrics. EPA-600/7-77-084 (NTIS PB-276489), U. S. Environmental Protection Agency, August 1977.

METRIC EQUIVALENTS

Readers more familiar with metric units may use the following to convert to that system.

Nonmetric	Multiply by	Yields metric
ft/min	0.00508	m/s
in. H_2O	249	Pa
lb/sq ft	3.28	kg/m^2
ft	0.305	m
lb	0.454	kg
ft^2	0.0929	m^2
lb/h	0.454	kg/h
acfm	0.0284	m^3/min

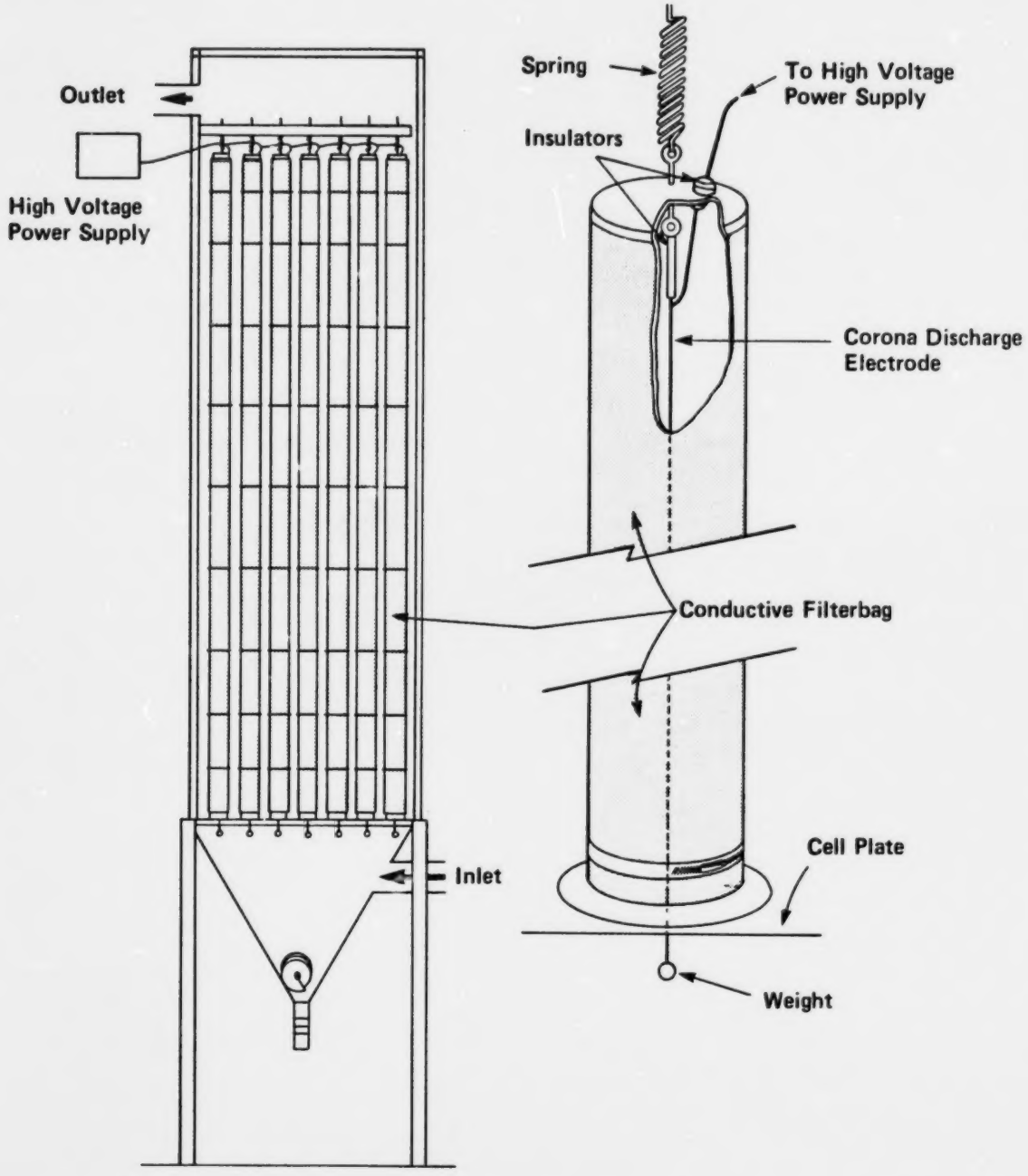

Figure 1. Advanced ESFF reverse-air configuration.

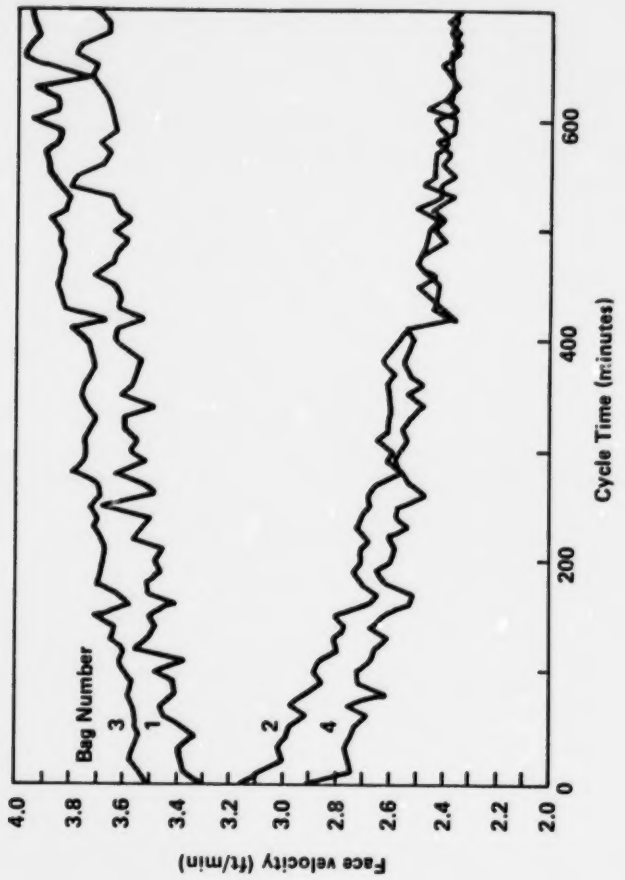

Figure 2. Individual bag flow data from ESFF pilot plant.

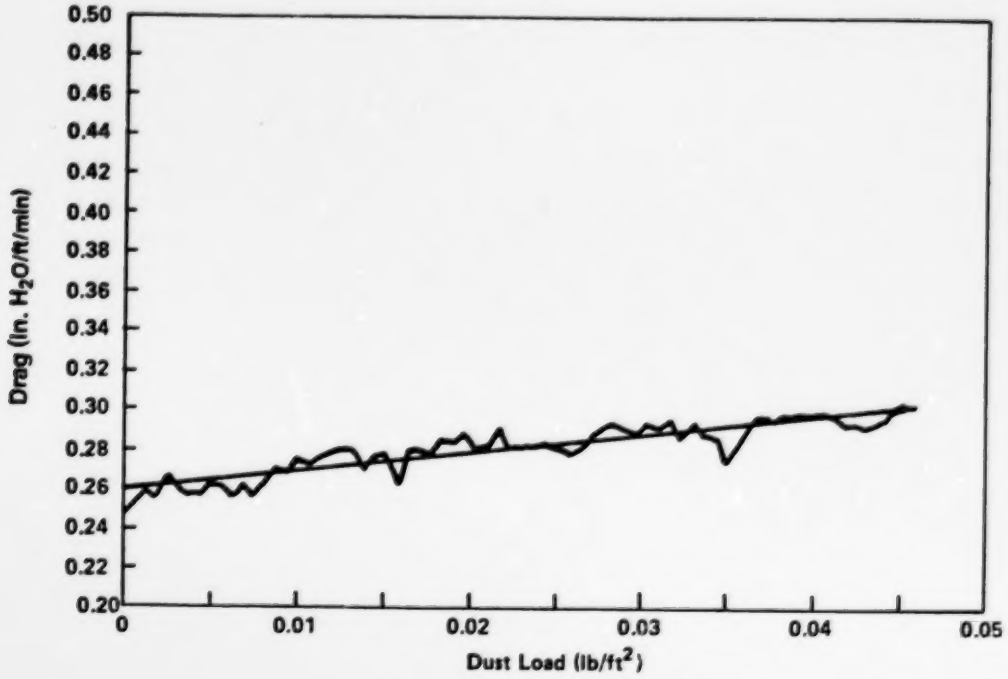

Figure 3. Drag correlation for bag No. 1 (ESFF).

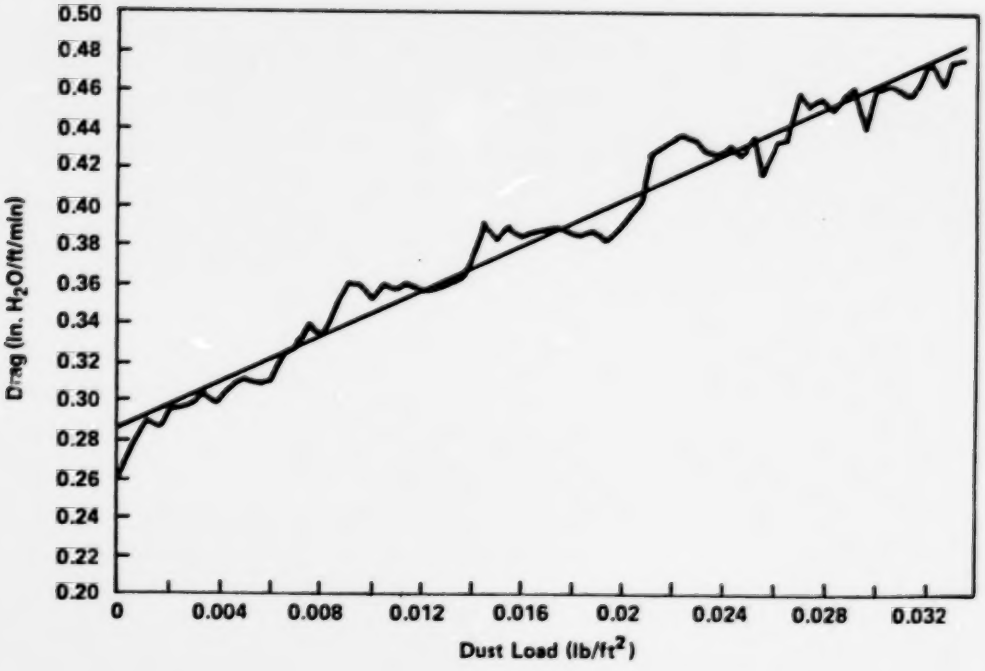

Figure 4. Drag correlation for bag No. 2 (conventional).

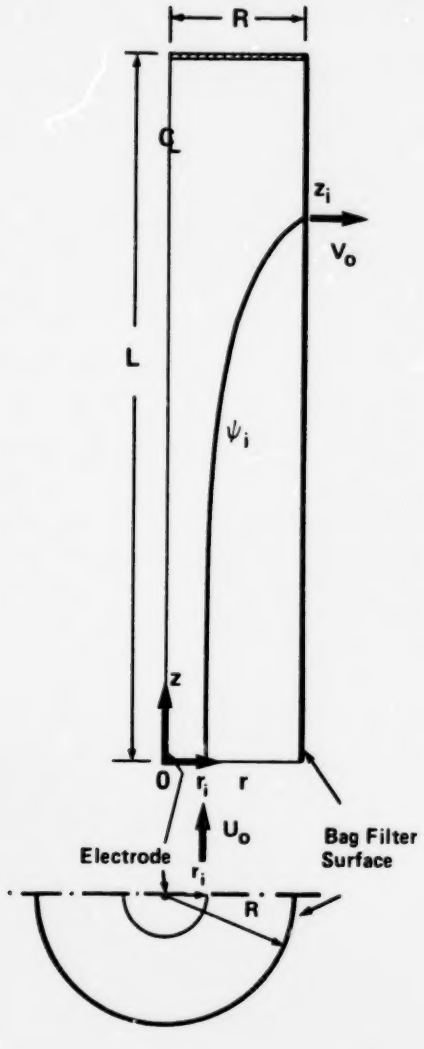

Figure 5. Advanced ESFF configuration.

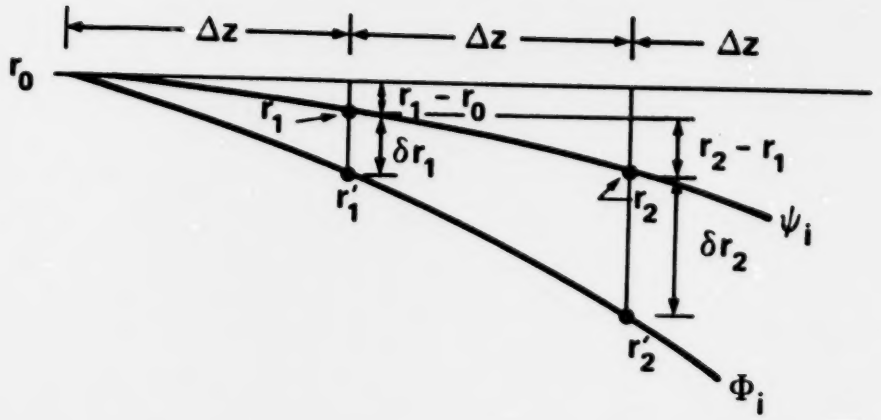

Figure 6. Illustration of increments used to compute particle trajectories.

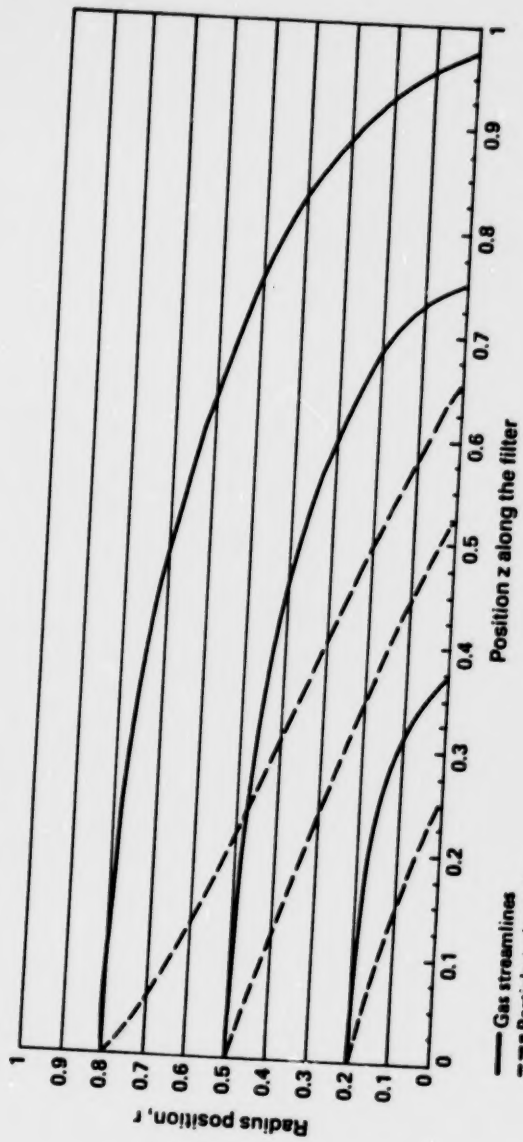

Figure 7. Gas and particle streamlines.

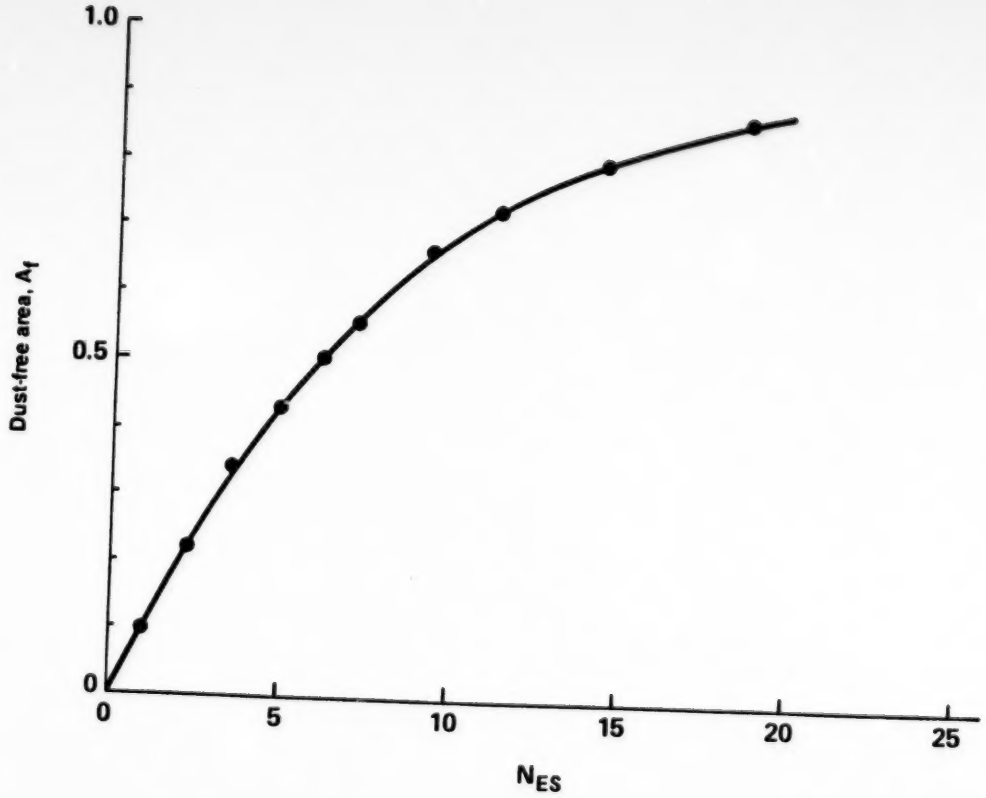

Figure 8. Dust-free area versus ES number.

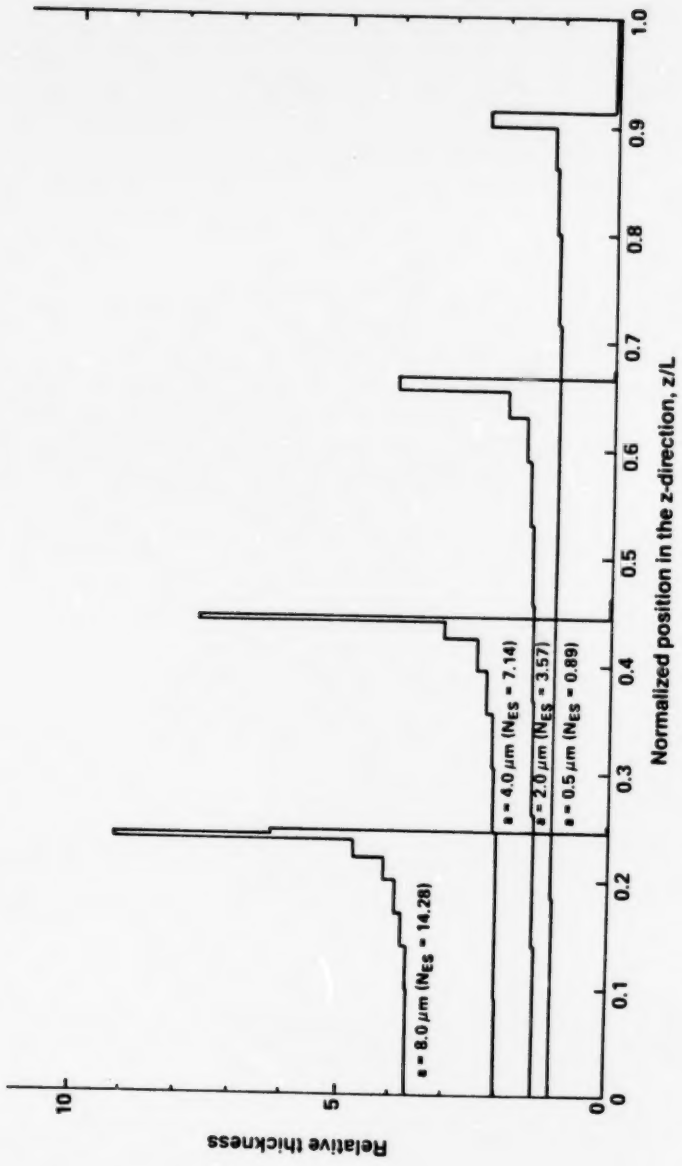

Figure 9. Dust layer distribution.

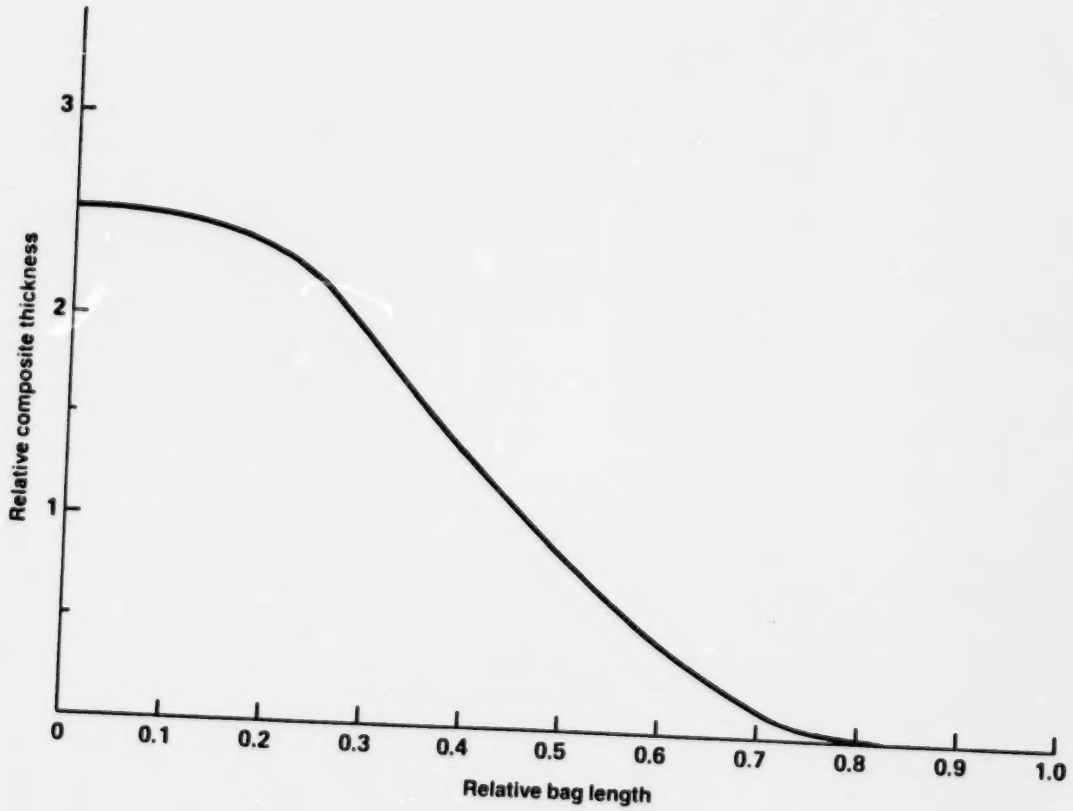

Figure 10. Relative thickness versus relative bag length.